Biol. Cybern. 72, 261–277 (1995)

Biological Cybernetics

Motion anisotropies and heading detection

Markus Lappe[1], **Josef P. Rauschecker**[2]

[1] Department of Zoology and Neurobiology, Ruhr University Bochum, D-44780 Bochum, Germany
[2] Laboratory of Neuropsychology, NIMH, Bethesda, MD 20892-4415, USA

Received: 1 April 1994/Accepted in revised form: 4 August 1994

Abstract. In motion-processing areas of the visual cortex in cats and monkeys, an anisotropic distribution of direction selectivities displays a preference for movements away from the fovea. This 'centrifugal bias' has been hypothetically linked to the processing of optic flow fields generated during forward locomotion. In this paper, we show that flow fields induced on the retina in many natural situations of locomotion of higher mammals are indeed qualitatively centrifugal in structure, even when biologically plausible eye movements to stabilize gaze on environmental targets are performed. We propose a network model of heading detection that carries an anisotropy similar to the one found in cat and monkey. In simulations, this model reproduces a number of psychophysical results of human heading detection. It suggests that a recently reported human disability to correctly identify the direction of heading from optic flow when a certain type of eye movement is simulated might be linked to the noncentrifugal structure of the resulting retinal flow field and to the neurophysiological anisotropies.

1 Introduction

The changing pattern of light arriving in the eyes of an animal moving through the world is a viable source of information about the movement. When the position of the eyes in the head and the position of the head with respect to the body is fixed, the 'optic flow' emanates from a singularity called the 'focus of expansion'. Under these conditions, the retinal projection of this singularity immediately indicates the direction of heading (Gibson 1950). However, the optic flow pattern on the retina is profoundly influenced by the eye movements of the observer (Regan and Beverly 1982), since it is the superposition of the centrifugal expansion pattern generated by a forward translation with the rotational pattern generated by the eye movement. Thus, to acknowledge the difference and to prevent confusion, it seems advisable to call the combined flow pattern the 'retinal flow'. The retinal flow then contains both propriospecific and exterospecific components and does not simply hint at the direction of heading with the singular point of a centrifugal motion (Koenderink and van Doorn 1981; Regan and Beverly 1982).

Nevertheless, the visual system of higher mammals does seem to put special emphasis on centrifugal motion. In the visual cortex of cats, a majority of cells in an area specialized for motion processing favor movements away from the area centralis (Rauschecker et al. 1987). This centrifugal bias is present in areas PMLS and PLLS (the posteromedial and posterolateral part of the cat's lateral suprasylvian cortex) and independent of early visual exposure (Brenner and Rauschecker 1990). It has been hypothetically linked to the processing of optic flow fields during egomotion (Rauschecker 1988). The finding of an overrepresentation of centrifugal motion has been confirmed for the representation of the peripheral visual field in the middle temporal area (MT) in monkey cortex (Albright 1989), the probable equivalent of cat PMLS. However, it is carried only by a subclass of MT neurons, the 'tuned cells', which also exhibit an increase in preferred speed with increasing eccentricity of their receptive field centers (Lagae et al. 1993). This trend has been reported previously for MT (Maunsell and Van Essen 1983) as well as for PMLS and PLLS (Rauschecker et al. 1987). It is highly consistent with the hypothesis of an involvement in optic flow processing. However, areas PMLS and MT also contain a fair number of neurons with preferred directions arranged circularly around the fovea. In the MT, neurons with a broadband speed response show such a specialization for movements orthogonal to the centrifugal motions preferred by the tuned cells (Lagae et al. 1993). Similar, trends can already be seen in the distribution of preferred directions earlier described in PMLS (Rauschecker et al. 1987). In PMLS, such cells are segregated from those preferring centrifugal motion, with centrifugal cells located anterior to circular motion cells (Sherk and Mulligan, personal communication). Also in cat area 18, a differentiation between centrifugal and circular direction preferences exists (Bauer et al. 1989).

Correspondence to: M. Lappe

Psychophysically, a perceptual bias for centrifugal motion has been reported by a number of authors (Ball and Sekuler 1980; Fahle and Wehrhahn 1991; Georgeson and Harris 1978), but an enhanced ability to detect centripetal motion instead has also been described (Edwards and Badcock 1993; Raymond 1994), depending on the stimulus used. The difference has been attributed to two different perceptual systems, one concerned with optic flow processing, the other with object motion and reaching (Mateeff et al. 1991) or figure/ground segmentation (Raymond 1994). Support for this differentiation also comes from the observation that centrifugal and centripetal movements are perceived differently. When a rigid object moves towards the observer (centrifugal motion), it is perceived rigidly, whereas when it moves away from the observer (centripetal motion), a nonrigid two-dimensional percept occurs (Perrone 1986). In the area of optic flow processing, however, experiments on the visual control of stance have demonstrated a specialization of different retinal regions to different flow patterns more clearly. Compensatory sway is strongest when radial flow is presented in the visual field center and lamellar flow in the periphery (Stoffregen 1985, 1986). Human heading detection from optic flow during pure ego-translations without confounding eye movements is most accurate when the focus of expansion is in the center of the visual field and decreases as it is positioned more peripherally (Warren and Kurtz 1992).

In this paper, we will demonstrate that a neural specialization to motion away from the fovea, i.e. a centrifugal and circular arrangement of movement detectors, can be an efficient design for detecting the direction of heading even when biologically plausible eye movements are performed during locomotion. First, in Sect. 2, we will analyse retinal flow fields induced in various situations that typically occur during the locomotion of higher mammals and that have been used in testing human heading detection. We show that in situations in which humans have been found to succeed, the retinal flow has an overall centrifugal structure, while in cases where human subjects failed, it has not. In Sect. 3, we introduce a network model of heading detection from retinal flow that builds on cells similar to MT or PMLS neurons and generates optic flow selective cells with properties similar to neurons in the medial superior temporal area (MST) in monkey visual cortex (Lappe and Rauschecker 1993a, b). The model incorporates as anisotropy in its input layer similar to the anisotropies found in cat and monkey. In Sect. 4, we will compare the performance of the anisotropic network with that of a network with an isotropic distribution of direction preferences in simulations that are closely related to various studies of human heading detection. The anisotropic version of the network is able to reproduce the results of the human experiments. Specifically, the degradation of the accuracy in detection of the direction of heading from certain noncentrifugal flow fields (Crowell and Banks 1993; Royden et al. 1992; Warren and Kurtz 1992) is yielded by the anisotropic, but not by the isotropic model. Section 5 discusses the results.

Part of this study has been published previously in brief (Lappe and Rauschecker 1994).

2 Different patterns of retinal flow

Humans have been quite accurate in many studies of heading detection from retinal flow despite the confounding influence of eye movements (Cutting et al. 1992; Rieger and Toet 1985; van den Berg 1992; Warren and Hannon 1988, 1990). Errors in detecting the direction of heading from displays simulating observer translation and rotation average roughly between 1 and 2 deg of visual angle (Warren and Hannon 1988). Recently, however, Royden et al. (1992) suggested that this might be true only for small rotation rates. In their study, they presented optic flow displays simulating translation over a ground plane and added various amounts of eye rotation, either by requiring the subject to fixate a moving spot or by having the subject fixate a stationary spot and simulating the equivalent rotation in the display. They found large errors of 10 deg and more when the displays included simulated eye rotations of more than 1 deg/s. They concluded that humans need proprioceptive information and cannot perceive their heading from retinal flow alone. However, their displays contained an important difference to the displays used in an earlier study by Warren and Hannon (1990). While Royden et al. superimposed a constant rotation around a vertical axis onto a translational optic flow, Warren and Hannon simulated situations where the subjects fixated a target that was rigidly attached to the ground plane, albeit with much smaller rotation rates. Using this same paradigm, van den Berg found much more accurate heading judgements even with rotation rates exceeding 5 deg/s (van den Berg 1993). Therefore, it seems that the human ability to detect the direction of heading from optic flow displays not only depends on the speed but also on the exact nature of he eye movement, which heavily influences the structure of the retinal flow.

The structure of the retinal flow field is determined by the movement parameters of the observer and by the spatial layout of his visual environment. In the following, we present a mathematical analysis of some exemplary situations that a human or animal observer might be confronted with naturally and that have been used in the human heading detection studies mentioned above. Three cases will be considered: First we briefly recapitulate the simple case in which no eye movements occur at all (2.1). Then we present an extensive analysis of a situation that is probably most natural of all (2.2), namely that the environment consists of a ground plane, and the observer keeps his eyes fixed on some visual feature on the ground plane during his movement. The third type of eye movement we will consider (2.3) is a rotation around a vertical axis during ego-translation over a ground plane. Such an eye movement might correspond to the tracking of an object located at some distance from the observer and potentially moving on its own. We will show that situations 2.2 and 2.3 result in very different retinal flow fields. In section 2.4 we will discuss the retinal flow fields experienced under the same self-movements in environments other than a ground plane.

Mathematically, the retinal flow field is obtained by projecting the motion of objects in the three-dimensional

(3D) world onto a 2D image plane (Longuet-Higgins and Prazdny 1980; Prazdny 1980). We assume a static environment so that all points in space share the same six motion parameters relative to the observer: the translation $\mathbf{T} = (T_x, T_y, T_z)^t$ and the rotation $\mathbf{\Omega} = (\Omega_x, \Omega_y, \Omega_z)^t$. In a cartesian coordinate system centered in the nodal point of the observer's eye, the 3D motion of point $\mathbf{R} = (X, Y, Z)^t$ is

$$\mathbf{V} = -\mathbf{T} - \mathbf{\Omega} \times \mathbf{R}. \tag{1}$$

Under perspective projection with focal length f, point $\mathbf{R}$ is transformed into

$$\mathbf{r} = \begin{pmatrix} x \\ y \end{pmatrix} = f \begin{pmatrix} X/Z \\ Y/Z \end{pmatrix}. \tag{2}$$

The 2D vector $\mathbf{r}$ describes a point in the image plane. The image plane is parallel to the (X, Y)-plane and positioned at a distance f from the origin. The retinal flow $\boldsymbol{\theta}(x, y)$ at point $\mathbf{r} = (x, y)^t$ is the motion of $\mathbf{r}$ on the image plane:

$$\boldsymbol{\theta}(x, y) = \frac{\mathrm{d}\mathbf{r}}{\mathrm{d}t} = f \begin{pmatrix} (\dot{X}Z - X\dot{Z})/Z^2 \\ (\dot{Y}Z - Y\dot{Z})/Z^2 \end{pmatrix}.$$

With (1) and (2), the retinal flow $\boldsymbol{\theta}(x, y)$ can be written as the sum of two terms, one depending on the observer's translation and one depending on his rotation:

$$\boldsymbol{\theta}(x, y) = \frac{1}{Z} \begin{pmatrix} -fT_X + xT_Z \\ -fT_Y + yT_Z \end{pmatrix} + \begin{pmatrix} \frac{xy}{f}\Omega_X - \left(f + \frac{x^2}{f}\right)\Omega_Y + y\Omega_Z \\ \left(f + \frac{y^2}{f}\right)\Omega_X - \frac{xy}{f}\Omega_Y - x\Omega_Z \end{pmatrix}. \tag{3}$$

2.1 Retinal flow during pure translations

The simplest type of movement that may occur is that of a pure translation without any eye movements. In this case, $\mathbf{\Omega} = 0$, and the flow becomes

$$\boldsymbol{\theta}(x, y) = \frac{1}{Z} \begin{pmatrix} -fT_X + xT_Z \\ -fT_Y + yT_Z \end{pmatrix}. \tag{4}$$

It is well known that for a pure translation, the retinal flow is characterized by a focus of expansion. The retinal location of the focus of expansion is

$$\mathbf{s}_0 = \frac{f}{T_Z} \begin{pmatrix} T_X \\ T_Y \end{pmatrix}. \tag{5}$$

This is exactly the direction of heading in retinal coordinates, i.e. the projection of $\mathbf{T}$ onto the image plane. All retinal motion is radially away from this singularity. An example in which the observer moves on top of a ground plane can be seen in Fig. 1a.

2.2 The retinal flow field during fixation of a ground plane element

Let us now turn to a more interesting case. When the observer fixates a stationary target while he is moving, a rotational (eye) movement is required to keep the target fixed on the retina. The necessary rotation can be derived from the condition that the retinal movement of the target has to vanish. Assuming that the target is foveated, its 3D location can be written as $\mathbf{F} = (0, 0, Z_F)^t$. The condition for fixation reads:

$$\boldsymbol{\theta}(0, 0) = \frac{1}{Z_F} \begin{pmatrix} -fT_X \\ -fT_Y \end{pmatrix} + \begin{pmatrix} -f\Omega_Y \\ +f\Omega_X \end{pmatrix} = \begin{pmatrix} 0 \\ 0 \end{pmatrix}. \tag{6}$$

Choosing $\Omega_Z = 0$, we find

$$\mathbf{\Omega} = \frac{1}{Z_F}(T_Y, -T_X, 0)^t. \tag{7}$$

The retinal flow then becomes

$$\boldsymbol{\theta}(x, y) = \frac{1}{Z} \begin{pmatrix} -fT_X + xT_Z \\ -fT_Y + yT_Z \end{pmatrix} + \frac{1}{Z_F} \begin{pmatrix} \frac{xy}{f}T_Y + \left(f + \frac{x^2}{f}\right)T_X \\ \left(f + \frac{y^2}{f}\right)T_Y + \frac{xy}{f}T_X \end{pmatrix}. \tag{8}$$

We are especially interested in a movement relative to a ground plane, and fortunately this is a situation simple enough to be treated mathematically. In the following, we will show that when the observer fixates a ground plane target, the retinal flow retains a qualitatively outward moving structure, provided that the difference between the fixation direction and the observer's translational heading is small. We use the help of dynamical systems theory, which has been successfully applied to optic flow fields by Verri et al. (1989). Under certain assumptions (Verri et al. 1989) about the environment, the flow field can be regarded as the right-hand side of a planar system of differential equations:

$$\frac{\mathrm{d}}{\mathrm{d}t}\mathbf{r}(t) = \boldsymbol{\theta}(x, y).$$

The structure of the flow field can then be determined by characterizing the singular points of the phase portrait of this system. The singular points are obtained by solving $\mathrm{d}\mathbf{r}(t)/\mathrm{d}t = 0$. From (8), we find

$$\frac{1}{Z} \begin{pmatrix} -fT_X + xT_Z \\ -fT_Y + yT_Z \end{pmatrix} + \frac{1}{Z_F} \begin{pmatrix} \frac{xy}{f}T_Y + \left(f + \frac{x^2}{f}\right)T_X \\ \left(f + \frac{y^2}{f}\right)T_Y + \frac{xy}{f}T_X \end{pmatrix} = \begin{pmatrix} 0 \\ 0 \end{pmatrix}.$$

In a planar environment, the depth $Z(x, y)$ is given by

$$Z(x, y) = \frac{\mu f}{xE_X + yE_Y + fE_Z}, \tag{9}$$

where $\mathbf{E} = (E_X, E_Y, E_Z)^t$ denotes the normal vector to the plane, and μ is the distance between the plane and the origin. To find the singular points, we therefore have to solve:

$$(xE_X + yE_Y + fE_Z)(-fT_X + xT_Z) + fE_Z\left(\frac{xy}{f}T_Y + \left(f + \frac{x^2}{f}\right)T_X\right) = 0$$

$$(xE_X + yE_Y + fE_Z)(-fT_Y + yT_Z) + fE_Z\left(\left(f + \frac{y^2}{f}\right)T_Y + \frac{xy}{f}T_X\right) = 0$$

or

$$(xE_X + yE_Y)(-fT_X + xT_Z) + xE_Z(xT_X + yT_Y + fT_Z) = 0 \tag{10}$$

$$(xE_X + yE_Y)(-fT_Y + yT_Z) + yE_Z(xT_X + yT_Y + fT_Z) = 0 \tag{11}$$

Obviously,

$$\mathbf{s}_1 = \begin{pmatrix} 0 \\ 0 \end{pmatrix} \tag{12}$$

is a singular point. To find the other singular points we multiply (10) by y and (11) by x and subtract:

$$(xE_X + yE_Y)(xT_Y - yT_X) = 0. \tag{13}$$

In the following, we assume that neither of the two factors is zero for all x and y. Otherwise, if, for instance, $T_X = T_Y = 0$ the observer's movement is directed towards the fixation point. The rotation would then be zero, and the result a purely translational flow field as described in Sect. 2.1. On the other hand, if $E_X = E_Y = 0$, the ground plane would be parallel to the image plane. This requires the observer to look straight down towards his feet and move in some direction perpendicular to the line of sight. While a situation like this certainly gives rise to a very special retinal flow field, it is behaviorally insignificant, and we will not consider it here. Let us therefore first assume that $T_X \neq 0$. In this case,

$$y = \frac{T_Y}{T_X}x$$

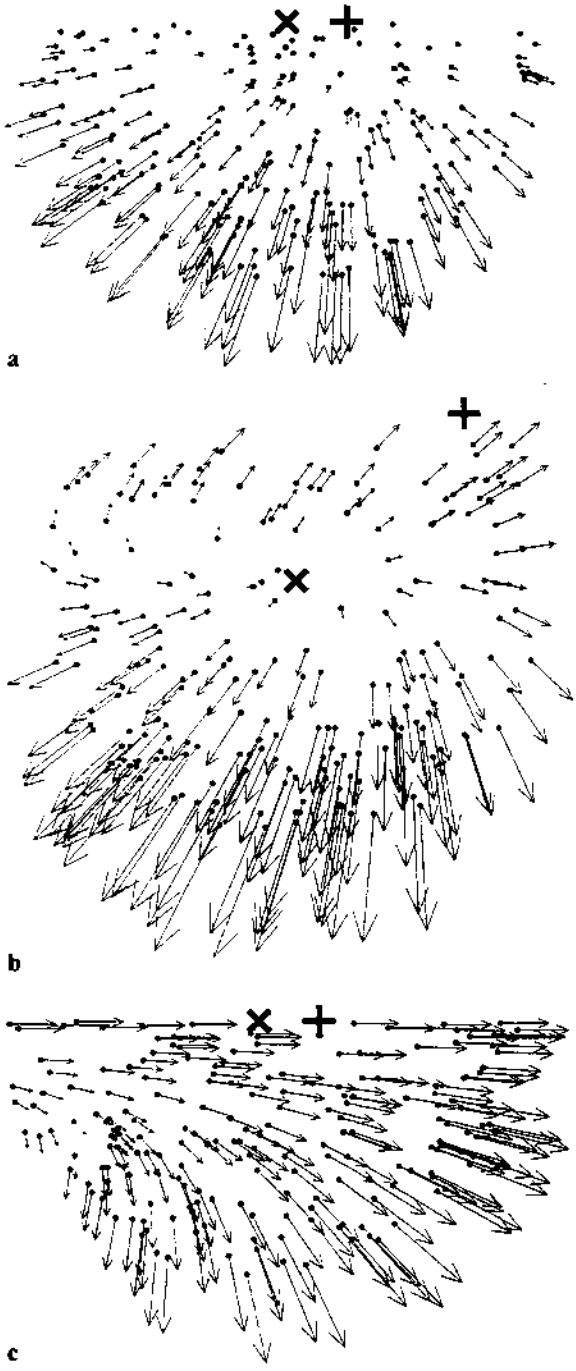

Fig. 1a–c. Three types of retinal flow fields that can be experienced during movement over a ground plane. In each picture, the direction of heading is indicated by a plus (+), while the fovea is marked by a cross (×). Note that these are observer-centered plots in which the fovea is always in the center. Visual field diameter is 34 deg. **a** A flow field generated by a pure translation without eye movements. It features a focus of expansion on the right side that coincides with the direction of heading. While, strictly speaking, all retinal movements radiate away from the focus of expansion, the overall structure is approximately centrifugal with respect to the fovea. **b** A retinal flow field that occurs when the observer fixates an element of the ground plane during egomotion. The eye movement necessary to fixate such a target gives rise to a rotational component in the flow field. The fixation target itself is projected onto the fovea. As a result, the center of the visual field contains a singular point. The direction of heading (+), on the other hand, is not a singular point any longer. However, the overall structure of the flow field is still largely centrifugal. **c** Retinal flow corresponding to a situation in which a constant eye rotation around a vertical axis is superimposed on the observer's translation. This might e.g. reflect the tracking of a moving object not affixed to the ground plane. Rotation rate is 3 deg/s, translational speed is 2 m/s. Both parameters are identical to those in **b**. Again the direction of heading (+) is not a singular point. The overall structure of the flow field, however, is quite different from the one shown in **b**. The individual movement vectors are arranged in a curved fashion, suggesting a movement along a curved path. The flow field contains many centripetal motion components. The flow field in **a** was calculated from (4) with $\mathbf{T} = (0.13, 0, -1.99)^t$. The required depth values $Z(x, y)$ at a number of randomly distributed positions $(x, y)^t$ were obtained from (9) with $\mathbf{E} = (0, 1, 0)^t$, $\mu = 1.6$ and $f = 1$. For the flow field in **b**, (8) and (9) were used with $\mathbf{T} = (0.37, 0.37, -1.93)^t$, $\mathbf{E} = (-0.12, 0.98, 0.16)^t$, $\mu = 1.6$, $Z_F = 10$ and $f = 1$. To obtain the flow field in **c**, (18) was used with $\mathbf{T} = (0.13, 0, -1.99)^t$, $\Omega = -0.05$, $\mu = 1.6$ and $f = 1$

Inserting this into (10) and observing that $x \neq 0$ (otherwise we would again obtain the first singular point $\mathbf{s}_1 = (0,0)$), we find

$$(T_X E_X + T_Y E_Y)(-fT_X + xT_Z) + E_Z(xT_X^2 + xT_Y^2 + fT_X T_Z) = 0. \quad (14)$$

For movements on top of a ground plane, the movement direction $\mathbf{T}$ and the plane normal $\mathbf{E}$ are orthogonal to each other, so that

$$T_X E_X + T_Y E_Y = -T_Z E_Z. \quad (15)$$

Therefore, (14) can be written as

$$-E_Z T_Z(-fT_X + xT_Z) + E_Z(xT_X^2 + xT_Y^2 + fT_X T_Z) = 0,$$

or

$$x(T_X^2 + T_Y^2 - T_Z^2) + 2fT_X T_Z = 0.$$

or

$$x(T^2 - 2T_Z^2) + 2fT_X T_Z = 0.$$

Thus, the second singular point is

$$\mathbf{s}_2 = -\frac{2fT_Z}{T^2 - 2T_Z^2}\begin{pmatrix} T_X \\ T_Y \end{pmatrix}. \quad (16)$$

To obtain the third singular point, we assume that $E_Y \neq 0$ and insert

$$y = -\frac{E_X}{E_Y}x$$

into (10):

$$xE_Z\left(xT_X - x\frac{E_X}{E_Y}T_Y + fT_Z\right) = 0.$$

We find the third singular point

$$\mathbf{s}_3 = \frac{fT_Z}{T_X E_Y - T_Y E_X}\begin{pmatrix} -E_Y \\ E_X \end{pmatrix}. \quad (17)$$

Let us now evaluate the structure of each of the singular points in turn by looking at the linearization of the system in the neighborhood of singular point. The retinal flow field around a singular point $\mathbf{s}_i$ is determined (Verri et al. 1989) by the two eigenvalues λ_1 and λ_2 of the matrix

$$\mathbf{M}_{ij} = \left.\frac{\partial \boldsymbol{\theta}(x,y)}{\partial \mathbf{r}}\right|_{\mathbf{r}=\mathbf{s}_i}.$$

The eigenvalues are conveniently computed from

$$\lambda^2 - \mathrm{TrM}\lambda + \mathrm{DetM} = 0,$$

where TrM and DetM are the trace and the determinant of M. With $Z(x,y)$ given by (9), we can calculate the elements of $\mathbf{M}$ from (8):

$$\mathbf{M}_{11} = \frac{1}{\mu f}(2(E_X T_Z + E_Z T_X)x + (E_Y T_Z + E_Z T_Y)y + f(E_Z T_Z - E_X T_X))$$

$$\mathbf{M}_{12} = \frac{1}{\mu f}((E_X T_Z + E_Z T_X)y - fE_X T_Y)$$

$$\mathbf{M}_{21} = \frac{1}{\mu f}((E_Y T_Z + E_Z T_Y)x - fE_Y T_X)$$

$$\mathbf{M}_{22} = \frac{1}{\mu f}(2(E_Y T_Z + E_Z T_Y)y + (E_X T_Z + E_Z T_X)x + f(E_Z T_Z - E_Y T_Y))$$

For the first singular point $\mathbf{s}_1 = (0,0)^t$ we find

$$\mathrm{TrM} = \frac{1}{\mu}(2E_Z T_Z - E_X T_X - E_Y T_Y),$$

or with (15)

$$\mathrm{TrM} = \frac{3}{\mu}E_Z T_Z.$$

The determinant of $\mathbf{M}$ at $\mathbf{s}_1 = (0,0)^t$ is

$$\mathrm{DetM} = \frac{1}{\mu^2}E_Z T_Z(E_Z T_Z - E_X T_X - E_Y T_Y) = \frac{2}{\mu^2}E_Z^2 T_Z^2.$$

Therefore, the eigenvalues are

$$\lambda_1 = \frac{1}{\mu}E_Z T_Z, \quad \text{and} \quad \lambda_2 = \frac{2}{\mu}E_Z T_Z.$$

Since both eigenvalues are real and of the same sign, the singular point is a node. Forward locomotion implies that T_Z and E_Z are both negative. Hence, the singular point is an unstable node, similar to a focus of expansion. The retinal motion is directed away from the singular point.

For the second singular point, (16), lengthy but straightforward calculations result in

$$\mathrm{TrM} = -\frac{3}{\mu}E_Z T_Z$$

and

$$\mathrm{DetM} = \frac{2}{\mu^2}E_Z^2 T_Z^2.$$

The eigenvalues are

$$\lambda_1 = -\frac{1}{\mu}E_Z T_Z \quad \text{and} \quad \lambda_2 = -\frac{2}{\mu}E_Z T_Z.$$

Thus, the second singular point is a stable node, with retinal motion going towards it, similar to a focus of

contraction. Finally, for the third singular point (17), straightforward calculations give

$$\mathrm{TrM} = 0$$

and

$$\mathrm{DetM} = -\frac{1}{\mu^2} E_Z^2 T_Z^2.$$

Since the eigenvalues

$$\lambda_1 = \frac{1}{\mu} E_Z T_Z \quad \text{and} \quad \lambda_2 = -\frac{1}{\mu} E_Z T_Z$$

are of opposite sign, the third singular point is a saddle with retinal motion going towards it along one axis and away from it along another.

The structure of the retinal flow field can be further evaluated as a function of the eccentricity ε of the direction of heading, i.e. the angle between $\mathbf{T}$ and the Z-axis, the direction of gaze. If $\varepsilon < 45°$, the second singular point is not visible, since it would be the projection of a point lying behind the observer. To clarify this, we compute the depth $Z(s_2)$ of the second singular point using (9):

$$Z(s_2) = \frac{\mu f}{\dfrac{-2T_Z(E_X T_X + E_Y T_Y)}{T^2 - 2T_Z^2} + f E_Z}.$$

With (15), $Z(s_2)$ can be written as

$$Z(s_2) = \frac{\mu}{E_Z} \frac{T^2 - 2T_Z^2}{T^2}.$$

Observing that $T_Z = T\cos(\varepsilon)$, we find

$$Z(s_2) = \frac{\mu}{E_Z}(1 - 2\cos^2(\varepsilon))$$

$$= -\frac{\mu}{E_Z}\cos(2\varepsilon).$$

Therefore, as long as $\varepsilon < 45°$, the depth $Z(s_2)$ is negative, and hence the singular point is not visible. Moreover, if ε is small, the third singular point is located in the far periphery of the visual field. This can be seen by computing $\delta = \arctan(f|\mathbf{s}_3|^{-1})$, the eccentricity of $\mathbf{s}_3$. We start out with

$$|\mathbf{s}_3| = f T_Z \sqrt{\frac{E_X^2 + E_Y^2}{E_X^2 T_Y^2 + E_Y^2 T_X^2 - 2E_X E_Y T_X T_Y}}.$$

Taking the square of (15) we know that

$$2E_X E_Y T_X T_Y = E_Z^2 T_Z^2 - E_X^2 T_X^2 - E_Y^2 T_Y^2.$$

Therefore, we can write

$$|\mathbf{s}_3| = f T_Z \sqrt{\frac{E_X^2 + E_Y^2}{(E_X^2 + E_Y^2)(T_X^2 + T_Y^2) - E_Z^2 T_Z^2}}.$$

Since $E_Z^2 = 1 - E_X^2 - E_Y^2$, this can be transformed into

$$|\mathbf{s}_3| = f T_Z \sqrt{\frac{E_X^2 + E_Y^2}{(E_X^2 + E_Y^2)T^2 - T_Z^2}}$$

or

$$|\mathbf{s}_3| = \frac{f}{\sqrt{\dfrac{T^2}{T_Z^2} - \dfrac{1}{E_X^2 + E_Y^2}}}.$$

With $T_Z = T\cos(\varepsilon)$, and

$$\frac{1}{E_X^2 + E_Y^2} = \frac{1}{1 - E_Z^2} = \frac{Z_F^2}{Z_F^2 - \mu^2}$$

we finally have

$$\delta = \arctan\left(\frac{1}{\sqrt{\dfrac{1}{\cos^2(\varepsilon)} - \dfrac{Z_F^2}{Z_F^2 - \mu^2}}}\right).$$

Under natural conditions of forward locomotion as well as in the simulations used in many psychophysical experiments, the fixation point is located at some distance of several eye heights away from the observer. For $Z_F \gg \mu$, the above expression becomes

$$\delta = \arctan\left(\frac{1}{\sqrt{\dfrac{1}{\cos^2(\varepsilon)} - 1}}\right).$$

Since

$$\sqrt{\frac{1}{\cos^2(x)} - 1} = \tan(x)$$

the eccentricity of the third singular point is approximately

$$\delta = 90° - \varepsilon.$$

Thus, as long as $\mathbf{T}$ deviates only by a small amount from the straight-ahead direction, the third singular point is located in the far periphery and barely visible.

Let us summarize the results of this section: When the observer moves on top of a ground plane and fixates a stationary target that itself is an element of the ground plane, the retinal flow field possesses at most three singular points. The first one is an unstable node located in the center of the visual field. It gives rise to retinal motions away from the fovea. The remaining two singular points are a stable node and a saddle. If the eccentricity of the direction of heading is small ($\varepsilon < 45°$), the stable node is not visible, and the saddle is located in the peripheral visual field. The retinal flow field is then governed by the node in the center. Its radial structure is deformed, however, in the direction where the saddle is located. In sum, the retinal flow field still resembles an outflow from the fovea, but variations of the local directions of motion occur between the fovea and the retinal location of the saddle. An example flow field is depicted in Fig. 1b.

2.3 Retinal flow with superimposed rotation

The structure of the retinal flow field is fundamentally different when a translational movement over a ground

plane is combined with an arbitrary rotation around an axis perpendicular to the ground plane. This situation might occur, for instance, when a moving object is tracked. It can be described by the following choice of parameters in (3) and (9):

$\mathbf{E} = (0, 1, 0)^t$,

$\mathbf{\Omega} = (0, \Omega, 0)^t$,

$\mathbf{T} = (T_X, 0, T_Z)^t$.

With these parameters, the retinal flow becomes:

$$\boldsymbol{\theta}(x, y) = \frac{y}{\mu f}\begin{pmatrix} -fT_X + xT_Z \\ yT_Z \end{pmatrix} + \begin{pmatrix} -\left(f + \frac{x^2}{f}\right)\Omega \\ -\frac{xy}{f}\Omega \end{pmatrix}. \quad (18)$$

Solving $\boldsymbol{\theta}(x, y) = 0$ yields only one singular point:

$$\mathbf{s}_4 = \begin{pmatrix} -\frac{fT_Z}{T_X} \\ -\frac{\mu f \Omega}{T_X} \end{pmatrix}.$$

The Jacobian $\mathbf{M}$ at $\mathbf{s}_4$ is

$$\mathbf{M} = \begin{pmatrix} \frac{\Omega T_Z}{T_X} & -\frac{T_X^2 + T_Z^2}{\mu T_X} \\ -\frac{\mu \Omega^2}{T_X} & \frac{\Omega T_Z}{T_X} \end{pmatrix}.$$

From this, we find

$\mathrm{Tr}\mathbf{M} = 0$

and

$\mathrm{Det}\mathbf{M} = \Omega^2$.

The eigenvalues are

$\lambda_{1/2} = \pm i\Omega$

and the singular point is a center with retinal motions circulating around it. Notice, however, that if T_X and Ω are of opposite sign, the singular point is not visible at all, but rather lies on a part of the ground plane that is behind the observer. This can immediately be seen by observing that $y_4 > 0$ in this case. Also, since $x_4 = T_Z/T_X = \cot(\varepsilon)$, the singular point is located in the periphery as long as the heading eccentricity ε is small. In summary, the retinal flow field in this situation is not radial. Instead, the individual dot movements are arranged in a curved fashion, as shown in Fig. 1c. A similar retinal flow field can be experienced when the observer moves along a curved path without moving his eyes.

2.4 Other environments

As long as the environment is smooth and differentiable, the retinal flow of any moving surface can be locally approximated by that of a suitably oriented plane. With multiple objects present in the field of view, however, the retinal flow can be very complicated and contain many different singularities and even limit cycles (Verri and Aicardi 1990; Verri et al. 1989). Nevertheless, for human heading detection to function, the environment does not have to be smooth and differentiable, as has been demonstrated by experiments simulating movement through a cloud of randomly positioned dots (Warren and Hannon 1990). In this situation, the mathematical analysis along the lines of dynamical systems theory cannot be performed. Since the distance of an individual dot from the observer's eye is a random variable, the structure of the retinal flow field becomes random itself. In an environment containing large depth differences near the line of sight, inward motion on the retina can occur even when the eye rotation is due to the fixation of a stationary object (Cutting et al. 1992).

Before, in a ground plane environment, we have differentiated between a situation in which the observer fixates a target located on the plane and the situation in which a constant rotation around a vertical axis is added to the translational movement of the observer. In a cloud-like environment, this differentiation is difficult. As long as the eye movement is directed away from the direction of heading, one can always construct a stationary dot at a suitable distance from the observer that, when fixated during egomotion, induces the desired rotation. This is true, however, only for an instantaneous flow field, taken at one moment in time. In a series of successive flow fields, in contrast, fixation of a stationary dot would result in an increase in rotation rate over time.

In a cloud-like environment, the overall structure of the retinal flow depends on the relation between $\mathbf{T}$ and $\mathbf{\Omega}$, because only the translational part of the retinal flow is depth-dependent, whereas the rotational part is independent of $Z(x, y)$. As an illustration, see the examples in Fig. 2. For the same rotation rate of 3 deg/s, a translational speed of 0.5 m/s results in a practically unidirectional flow pattern in Fig. 2c, while at a translational speed of 3.0 m/s, the flow pattern contains a significant amount of centrifugal motion (Fig. 2b).

3 A network model of heading detection

In this section, we introduce a network model of heading detection that is especially well suited to work with centrifugal flow fields and is in concordance with neurophysiological data from cortical motion processing areas in higher mammals. The model consists of two layers of neurons. In the first layer, the retinal flow is represented by the activities of direction-selective neurons at a number of visuospatial locations. These neurons are modelled after cells in visual cortical areas PMLS in cat or MT in monkey. They respond maximally when a visual feature is swept through their receptive field along a certain preferred direction. They do not respond to movements in the opposite direction. For directions in between, they respond to a varying degree according to the angle between the direction of the movement and the preferred

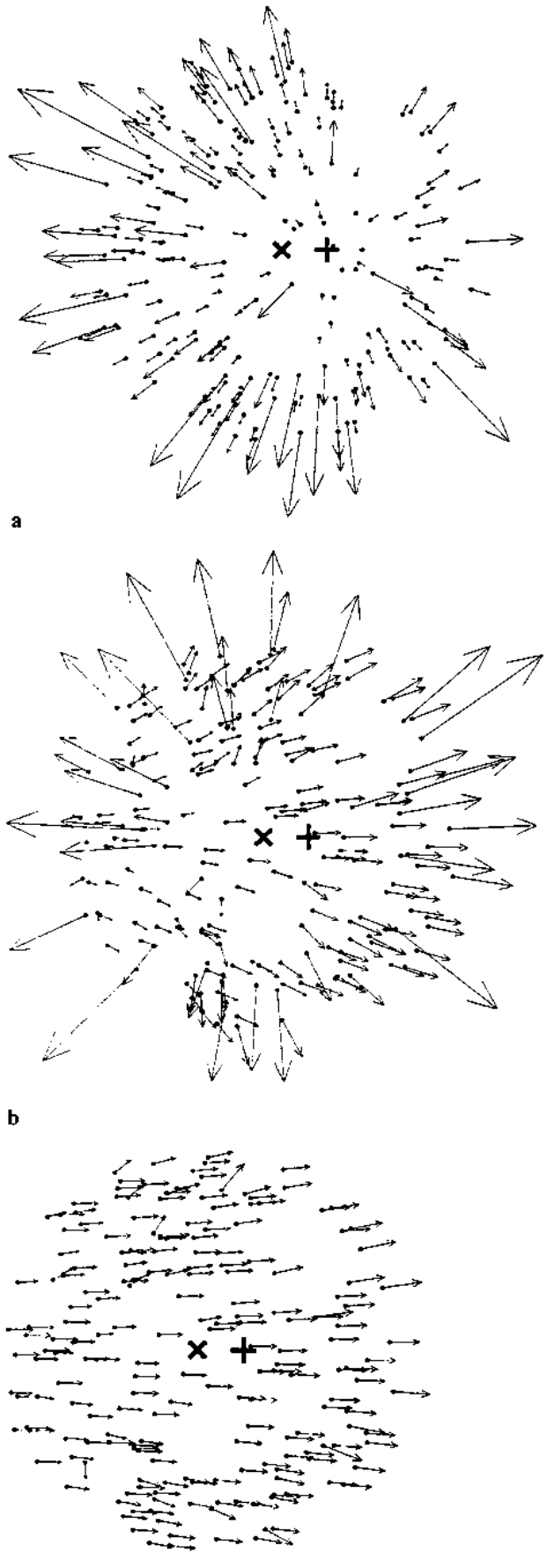

direction. Since one such cell alone cannot signal the 2D direction of motion of a visual object on the retina by itself (Marr and Ullman 1981), we employ a population encoding of each retinal flow vector by a small group of neurons with the same spatial receptive field positions but different preferred directions. This is biologically plausible and has already been proposed as the output of a neural network modelling the visual motion pathway between retina and area MT (Wang et al. 1989). Here we are not concerned with how the retinal flow field may be derived from the luminance changes on the retina, which is a complicated computational problem in its own right (Verri and Poggio 1989). Several models for this task have been introduced so far (Bülthoff et al. 1989; Hildreth 1984; Perrone 1990; Reichardt 1969; Uras et al. 1988; Verri et al. 1992; Werkhoven and Koenderink 1990; Yuille and Grzywacz 1988). Instead, we start out with a suitably simple form of population encoding of the motion vectors. In the isotropic version of the network, we use four neurons to represent a single retinal motion vector $\boldsymbol{\theta}_i$ as

$$\boldsymbol{\theta}_i = \sum_{k=1}^{4} s_{ik}\mathbf{e}_{ik}. \tag{19}$$

The preferred directions $\mathbf{e}_{ik} = (\cos((\phi_0 + \pi k/2), \sin((\phi_0 + \pi k/2))^t$ are equally spaced around ϕ_0, the direction of a line connecting the center of the receptive field of a neuron with the fovea. A neuron's response to a flow vector of direction ϕ_i and speed θ_i is given by the tuning curve

$$s_{ik} = \begin{cases} \theta_i \cos(\phi_i - (\phi_0 + \pi k/2)) \\ \quad \text{if } \cos(\phi_i - (\phi_0 + \pi k/2)) > 0 \\ 0 \\ \quad \text{otherwise} \end{cases}$$

In a modified version of the network, we account for the anisotropies found in PMLS and MT with respect to centrifugal and circular motion directions. In our model, this is simply done by omitting all neurons with centripetal preferred directions. As a result, movements that contain a centripetal component are misrepresented in the first layer of the network. Movements without a centripetal component, on the other hand, are represented correctly.

Fig. 2a–c. Three retinal flow fields generated by movements through a random 3D cloud of dots. The plus (+) marks the direction of heading, the cross (×) marks the fovea. Visual field diameter is 34 deg. The cloud extends from 2 to 40 m in depth. **a** Retinal flow of a pure translation without eye movements. The focus of expansion (+) gives the direction of heading. Translational speed is 3 m/s. **b** and **c** A rotation around a vertical axis is superimposed. Rotation rate equals 3 deg/s. In **b**, the translational speed is 3 m/s, while in **c** the observer moves at only 0.5 m/s. In the latter case, the flow field is basically lamellar, whereas in the former, it still contains a fair number of centrifugal movement vectors. All three examples were calculated from (3), with $f = 1$ and $Z(x, y)$ chosen randomly with equal probability between 2 and 40. The movement parameters for the different cases were $\mathbf{T} = (0.2, 0, -2.9)^t$, $\boldsymbol{\Omega} = (0, 0, 0)^t$ for **a**, $\mathbf{T} = (0.2, 0, -2.9)^t$, $\boldsymbol{\Omega} = (0, -0.05, 0)^t$ for **b**, and $\mathbf{T} = (0.033, 0, -0.48)^t$, $\boldsymbol{\Omega} = (0, -0.05, 0)^t$ for **c**

In the second layer of the network, possible translational heading directions $\mathbf{T}_j$ are represented by populations of neurons, the activities of which encode the likelihood that $\mathbf{T}_j$ is the correct direction of heading. Each population tests whether the retinal flow represented by the activities in the first layer is compatible with its preferred heading direction $\mathbf{T}_j$. It then adjusts its output population activity to reflect the degree of compatibility. The calculated direction of heading is given by the most active population, since neuronal populations preferring other directions are less excited. We would like to stress, however, that a single neuron in the output layer is itself not tuned to a certain preferred direction of heading. This tuning is rather a property of the whole population.

3.1 The subspace algorithm for heading detection

The calculation of the population activities representing the likelihood of a specific heading direction $\mathbf{T}_j$ is based on the subspace algorithm by Heeger and Jepson (1992). It carries out a least-square minimization over a set of possible heading directions. In the network model, the synaptic connections are chosen such that the neuronal populations in the second layer are maximally excited when the least-square error function is minimal. To give a brief summary of the subspace algorithm (Heeger and Jepson 1992), we write the retinal flow from (3) as

$$\boldsymbol{\theta}(x,y) = \frac{1}{Z(x,y)}\mathbf{A}(x,y)\mathbf{T} + \mathbf{B}(x,y)\boldsymbol{\Omega}, \tag{20}$$

with the matrices

$$\mathbf{A}(x,y) = \begin{pmatrix} -f & 0 & x \\ 0 & -f & y \end{pmatrix}$$

and

$$\mathbf{B}(x,y) = \begin{pmatrix} xy/f & -f - x^2/f & y \\ f + y^2/f & -xy/f & -x \end{pmatrix}.$$

$\mathbf{A}(x,y)$ and $\mathbf{B}(x,y)$ depend only on the image coordinates (x,y) and on the focal length f. The task of heading detection is to estimate $\mathbf{T}$, given a measured retinal flow $\boldsymbol{\theta}$. At first, one has to note that the unknown depth $Z(x,y)$ and $\mathbf{T}$ are multiplied together and cannot be determined independently. Therefore, $\mathbf{T}$ is regarded as a unit vector pointing in the direction of heading. Then the above equations contain six unknowns, $Z(x,y)$, two components of $\mathbf{T}$ and three components of $\boldsymbol{\Omega}$, but only two measurements, the two components of $\boldsymbol{\theta}(x,y)$. For the subspace algorithm, flow vectors from m different image points are combined into one matrix equation:

$$\boldsymbol{\Theta} = \mathbf{C}(\mathbf{T})_{\mathbf{q}}. \tag{21}$$

In this equation

$$\boldsymbol{\Theta} = (\boldsymbol{\theta}_1, \ldots, \boldsymbol{\theta}_m)^t$$

is a $2m$-dimensional vector consisting of the components of the m single image velocities, and

$$\mathbf{q} = (1/Z(x_1,y_1), \ldots, 1/Z(x_m,y_m), \Omega_x, \Omega_y, \Omega_z)^t$$

is an $(m+3)$-dimensional vector containing the unknown depth values of the m image points plus the three unknown components of $\boldsymbol{\Omega}$. The $2m \times (m+3)$ matrix $\mathbf{C}(\mathbf{T})$ is obtained by combining the matrices $\mathbf{A}(x_i,y_i)\mathbf{T}$ and $\mathbf{B}(x_i,y_i)$ of the individual image points in the following manner:

$$\mathbf{C}(\mathbf{T}) = \begin{pmatrix} \mathbf{A}(x_1,y_1)\mathbf{T} & \cdots & 0 & \mathbf{B}(x_1,y_1) \\ \vdots & \ddots & \vdots & \vdots \\ 0 & \cdots & \mathbf{A}(x_m,y_m)\mathbf{T} & \mathbf{B}(x_m,y_m) \end{pmatrix}. \tag{22}$$

The heading direction can then be recovered by minimizing the residual function

$$R(\mathbf{T}) = \|\boldsymbol{\Theta}^t\mathbf{C}^{\perp}(\mathbf{T})\|^2,$$

where $\mathbf{C}^{-}(\mathbf{T})$ is a matrix spanning the orthogonal complement of $\mathbf{C}(\mathbf{T})$ (Heeger and Jepson 1992). $\mathbf{C}^{\perp}(\mathbf{T})$ is defined in the following way: Provided that the columns of $\mathbf{C}(\mathbf{T})$ are linearly independent, they form a basis of an $(m+3)$-dimensional subspace of the $\mathscr{R}^{2m}$, which is called the range of $\mathbf{C}(\mathbf{T})$. The remaining $(2m-(m+3))$-dimensional subspace is called the orthogonal complement of $\mathbf{C}(\mathbf{T})$. Every vector in the orthogonal complement of $\mathbf{C}(\mathbf{T})$ is orthogonal to every vector in the range of $\mathbf{C}(\mathbf{T})$. The matrix $\mathbf{C}^{\perp}(\mathbf{T})$ is composed of vectors that span the orthogonal complement of $\mathbf{C}(\mathbf{T})$.

3.2 Implementation of the subspace algorithm in the network model

The second layer of the network consists of a number of neuronal populations, each of which represents a certain heading direction $\mathbf{T}_j$. A single population j shall be maximally excited when

$$R_j(\mathbf{T}) = \|\boldsymbol{\Theta}^t\mathbf{C}^{\perp}(\mathbf{T}_j)\|^2 = 0.$$

This is accomplished in a two-step process. First, an individual neuron l from population j evaluates part of the argument of $R_j(\mathbf{T})$ by picking out one of the column vectors of $\mathbf{C}^{\perp}(\mathbf{T}_j)$, denoted by $\mathbf{C}_l^{\perp}(\mathbf{T}_j)$, and computing $\boldsymbol{\Theta}^t\mathbf{C}_l^{\perp}(\mathbf{T}_j)$. This only requires a simple summation. In the second step, several neurons with different connections are combined so that the sum of the activities of these neurons is maximal when $\boldsymbol{\Theta}^t\mathbf{C}_l^{\perp}(\mathbf{T}_j) = 0$. To compute $\boldsymbol{\Theta}^t\mathbf{C}_l^{\perp}(\mathbf{T}_j)$, the synaptic connections between a second layer neuron and its input neurons in the first layer have to be assigned specific values. In our model, this is not done by some learning rule but is predetermined by the algorithm. We start by randomly choosing m first-layer populations as input to one second-layer neuron. These neurons form the receptive field of the second-layer cell. The second-layer neuron computes its output u_{jl} via a sigmoid transfer function comparing the summated input received from the first-layer neurons to a threshold μ:

$$u_{jl} = g\left(\sum_{i=1}^{m}\sum_{k=1}^{4} J_{ijkl}s_{ih} - \mu\right). \tag{23}$$

Here J_{ijkl} denotes the strength of the synaptic connection between the lth output neuron in the second-layer population representing heading direction $\mathbf{T}_j$ and the kth input neuron in the first-layer population representing the optic flow vector $\boldsymbol{\theta}_i$. Since the neuron is supposed to compute $\boldsymbol{\Theta}^t \mathbf{C}_l^{\perp}(\mathbf{T}_j)$, we require:

$$\sum_{i=1}^{m} \sum_{k=1}^{4} J_{ijkl} s_{ik} = \boldsymbol{\Theta}^t \mathbf{C}_l^{\perp}(\mathbf{T}_j). \tag{24}$$

This means that for every image location i we have:

$$\sum_{k=1}^{4} J_{ijkl} s_{ik} = \boldsymbol{\theta}_i^t \begin{pmatrix} C_{l,2i-1}^{\perp}(\mathbf{T}_j) \\ C_{l,2i}^{\perp}(\mathbf{T}_j) \end{pmatrix}.$$

Substituting (19) yields:

$$\sum_{k=1}^{4} J_{ijkl} s_{ik} = \sum_{k=1}^{4} s_{ik} \mathbf{e}_{ik}^t \begin{pmatrix} C_{l,2i-1}^{\perp}(\mathbf{T}_j) \\ C_{l,2i}^{\perp}(\mathbf{T}_j) \end{pmatrix}.$$

The values of the synaptic strengths thus have to be:

$$J_{ijkl} = \mathbf{e}_{ik}^t \begin{pmatrix} C_{l,2i-1}^{\perp}(\mathbf{T}_j) \\ C_{l,2i}^{\perp}(\mathbf{T}_j) \end{pmatrix}.$$

With synaptic strengths like this, the input to the neuron already is a measure of how compatible $\mathbf{T}_j$ is with the sampled retinal flow. When $\boldsymbol{\Theta}$ is in the range of $\mathbf{C}(\mathbf{T}_j)$, i.e. when $\mathbf{T}_j$ is likely to be the correct direction of heading, the neuron receives a net input of zero. The following second step is concerned with the properties of the population of neurons representing a single heading direction $\mathbf{T}_j$. First, we consider a second neuron $u_{jl'}$ so that the sum of the activities of the two neurons is maximal when $\boldsymbol{\Theta}^t \mathbf{C}_l^{\perp}(\mathbf{T}_j) = 0$. Both neurons are connected to the same set of image locations but with complementary connection strengths satisfying $J_{ijkl'} = -J_{ijkl}$. Also, the threshold μ shall be slightly negative. Then the sum $u_{jl} + u_{jl'}$ of the two neurons' activities reaches its peak value when the input to both neurons is zero. This is a result of the maximum overlap of their complementary sigmoid transfer functions. However, such a pair of neurons still cannot signal the correct direction of heading. It only tests whether $\boldsymbol{\Theta}^t \mathbf{C}_l^{\perp}(\mathbf{T}_j) = 0$. Since $\boldsymbol{\Theta}$ is a function of both T_X and T_Y, this condition is fulfilled along a line in (T_X, T_Y)-space. The summed activities of the two neurons are maximal for all pairs of (T_X, T_Y) that fall along this line. Therefore, additional pairs of neurons are needed with different sets of inputs, i.e., different receptive fields, that test if $\boldsymbol{\Theta}^t \mathbf{C}_l^{\perp}(\mathbf{T}_j) = 0$. All of these neurons together form a single population that represents $\mathbf{T}_j$. The sum of all of their responses is maximal when $R_j(\mathbf{T}) = 0$. However, the arrangement of neurons in matched pairs with $J_{ijkl'} = -J_{ijkl}$ is not required when the number of neurons in the population is large. Then the randomness of the distribution of their inputs automatically results in maximum overlap of their individual transfer functions when the input to all neurons is zero.

3.3 Different constraints on eye movements

We have previously shown that different constraints imposed on the nature of the expected eye movements of the observer result in different response properties of the second-layer cells in simulations mimicking neurophysiological experiments (Lappe and Rauschecker 1993a). The neurons might respond to expansional, contractional, rotational, and translational random dot patterns, or alternatively only to a subset of these stimuli. Similarly, in monkey area MST, a variety of response selectivities have been found (Duffy and Wurtz 1991). Some cells are selective for only one retinal flow pattern, like for instance expansion (Saito et al. 1986; Tanaka et al. 1986; Tanaka and Saito 1989). Others respond to two or even three patterns. A single cell might, for example, favor contractions and clockwise rotations and unidirectional motion in a specific direction when tested with these stimuli one after another (Duffy and Wurtz 1991; Orban et al. 1992). Also, cells in MST have been shown to respond to superpositions of expansion and rotation that yield spiraling flow patterns (Graziano et al. 1994). A similar diversity of cell response selectivities can be achieved by the model when specializations to different types of eye movements are assumed. In the simulations described in this paper, we decided to use a mix of the various cell types generated by different eye movement constraints in our model. In the following, we give a brief overview over these cell types.

When a second-layer cell is formed without any constraints on the eye movements, as described in Sect. 3.2, it exhibits selectivities to expanding/contracting as well as to planarly translating dot patterns. It does not, however, select between clockwise or counterclockwise rotating patterns and thus might be termed a double-component cell (Lappe and Rauschecker 1993a). When we assume instead that the observer fixates an environmental object while he is moving, the eye rotation is related to the observer translation by (7), no matter whether the object is attached to a ground plane or is located at some arbitrary distance Z_F, as with a cloud-like environment. Note that in this framework a situation with no eye movements at all could be approximated by $Z_F \to \infty$. The retinal flow in the form suitable for the subspace algorithm (20) then becomes

$$\tilde{\boldsymbol{\theta}}(x,y) = \frac{1}{Z(x,y)} \mathbf{A}(x,y)\mathbf{T} + \frac{1}{Z_F} \tilde{\mathbf{B}}(x,y)\mathbf{T}$$

with

$$\tilde{\mathbf{B}}(x,y) = \begin{pmatrix} f + x^2/f & (xy)/f & 0 \\ (xy)/f & f + y^2/f & 0 \end{pmatrix}.$$

In analogy to (22), a new matrix

$$\tilde{\mathbf{C}}(\mathbf{T}) = \begin{pmatrix} \mathbf{A}(x_1,y_1)\mathbf{T} & \cdots & 0 & \tilde{\mathbf{B}}(x_1,y_1)\mathbf{T} \\ \vdots & \ddots & \vdots & \vdots \\ 0 & \cdots & \mathbf{A}(x_m,y_m)\mathbf{T} & \tilde{\mathbf{B}}(x_m,y_m)\mathbf{T} \end{pmatrix}$$

can be constructed. Synaptic connections and neural populations can then be formed with the procedure described in Sect. 3.2. If a single neuron is constructed in this way, it is selective for all three types of flow patterns. It exhibits broad directional tuning and responds selectively to expanding/contracting and rotating patterns

(Lappe and Rauschecker 1993a). It resembles a triple component cell in MSTd.

Another sensible constraint on eye movement is the assumption that the axis of rotation is parallel to the image plane. This would only rule out torsional components, which are not very likely to occur to a significant amount during normal fixation anyway. On the contrary, eye torsion often acts as a stabilizer of the retinal image, for instance, in counterrotations to small tilts of the head. Frontoparallel rotations are defined by $\Omega_Z = 0$. Inserting $\Omega_Z = 0$ into (20) yields

$$\hat{\boldsymbol{\theta}}(x,y) = \frac{1}{Z(x,y)}\mathbf{A}(x,y)\mathbf{T} + \hat{\mathbf{B}}(x,y)\begin{pmatrix}\Omega_X\\ \Omega_Y\end{pmatrix}$$

where

$$\hat{\mathbf{B}}(x,y) = \begin{pmatrix} xy/f & -(f+x^2/f)\\ f+y^2/f & -xy/f\end{pmatrix}$$

now is a 2×2 matrix. As a result

$$\hat{\mathbf{C}}(\mathbf{T}) = \begin{pmatrix} \mathbf{A}(x_1,y_1)\mathbf{T} & \cdots & 0 & \hat{\mathbf{B}}(x_1,y_1)\\ \vdots & \ddots & \vdots & \vdots\\ 0 & \cdots & \mathbf{A}(x_m,y_m)\mathbf{T} & \hat{\mathbf{B}}(x_m,y_m)\end{pmatrix}$$

is a $2m\times(m+2)$ matrix. A neuron that is constructed using $\hat{\mathbf{C}}(\mathbf{T})$ maximally responds to one direction of rotation and is less selective to expansions and unidirectional shifts (Lappe and Rauschecker 1993a). It is similar to a single-component rotation-selective cell.

4 Simulation results

In this section, we present simulations of the network which relate to some recent psychophysical experiments. We will show that an anisotropic version of the network yields results that are compatible with the psychophysical findings while the unmodified isotropic network does not.

The first simulations are concerned with the retinal eccentricity of the direction of heading under conditions of pure translation. Warren and Kurtz (1992) as well as Crowell and Banks (1993) performed experiments in which the retinal location of the focus of expansion was varied. Both groups found least errors in detecting the direction of heading when the focus of expansion was presented near the fovea. With increasing eccentricity of the focus of expansion, the heading errors increased, too. The authors agreed that this might reflect a specialization to radial motion patterns centered at the fovea.

Thereafter, we present simulations in which eye rotations are simulated. Three different experimental conditions are compared. Two of them simulate movement over a ground plane. In the first condition, the observer fixates an element of the ground plane, giving rise to an approximately centrifugal retinal flow field of the type described in Sect. 2.2. Such a stimulus has been used by several authors (Cutting et al. 1992; van den Berg 1992; Warren and Hannon 1990) who consistently found heading errors around 2 deg irrespective of varying amounts of rotation. In the second condition that we simulate, a rotation about a vertical axis is added to a translational movement, as described in Sect. 2.3. Using this stimulus, (Royden et al. 1992) found large heading errors of 10 deg or more, when the rotation rate exceeded 1 deg/s. Our third condition uses a cloud of randomly positioned dots extending from 2 to 40 meters in depth. An eye rotation about a vertical axis is added which might be regarded as the result of the fixation of a dot at a specific distance or as the fixation of a moving object. While this stimulus has been used by many authors, the obtained results vary. Warren and Hannon (1990) used small rotation rates ($\leqslant 0.7$ deg/s) together with high translational speeds (1.9 m/s) and found small errors (1.4 deg). Royden et al. (1992) found large errors (> 10 deg) using high rotation rates (2.5–5.0 deg/s) and a slow translational speed (0.5 m/s). Medium errors (2–4 deg) were obtained by van den Berg (1992), who paired high rotation rates (up to 6 deg/s) with high translational speeds (3.0 m/s). In addition to simulations varying the rotation rate, we therefore also performed simulations in which the translational speed was varied, while the rotation rate was held constant. Finally, while most of our simulations are designed to be compatible with the published psychophysical studies, we also performed simulations in which the visual field size was increased as compared with the psychophysical stimulations.

The standard parameters for the simulation were the following. The flow field input to the first layer consisted of 200 motion vectors randomly distributed inside a visual field of 34 deg in diameter. In the second layer, a 19×19 grid of cell populations was used covering 40×40 deg of heading eccentricity. A single population thus roughly covered a 2×2 deg patch of possible heading directions. Each population contained 20 pairs of neurons. Every neuron was connected to 30 randomly selected first-layer cell populations. The neurons within one second-layer population received input from different first-layer populations. Each simulation run computed the mean error by averaging over 100 trials with different, randomly chosen heading directions.

4.1 Eccentricity of the focus of expansion

In the first simulation, we tested the influence of the retinal eccentricity of the focus of expansion. The simulated environment consisted of a cloud of dots extending from 2 to 40 m in depth, and the movement was a pure translation with a speed of 1.9 m/s. No rotation was present. The network was run with heading directions that were constrained to lie on a circle of radius ε around the fovea. The heading eccentricity ε was varied between 2 and 18 deg of visual angle. In this simulation, the visual field had a diameter of 40 deg. The results are shown in Fig. 3. The mean error is plotted versus the rotation rate for both an isotropic distribution of direction preferences in the first layer and an anisotropic distribution that contained no preferred directions towards the fovea. With the anisotropic distribution of preferences, the mean error rises moderately as the eccentricity increases. This result is consistent with the

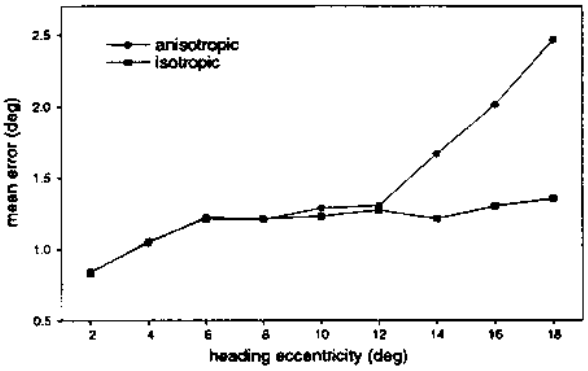

Fig. 3. Mean angular error in detecting the direction of heading of a pure translation as a function of the eccentricity ε of the focus of expansion. The simulations consisted of movement with 1.9 m/s through a cloud of dots extending from 2 to 40 m in depth. Each point is the mean of 100 network trials with different directions of heading constrained to lie on a circle of radius ε around the fovea. As ε increases, the error of the anisotropic network becomes progressively larger. With an isotropic distribution of direction preferences in the input layer, the error stays around 1 deg throughout the range of heading eccentricities tested

findings of Warren and Kurtz (1992) and Crowell and Banks (1993). The dependency of the mean error on the heading eccentricity is, however, not present in the isotropic version of the network.

4.2 Superimposed rotation vs fixation of a ground plane element

We compared the responses of the network to the two types of movements described in Sect. 2.2 and 2.3 and depicted in Fig. 1b,c. The ground plane was located 1.6 m below the nodal point of the simulated observer's eye. Translational speed was 1.9 m/s. The rotation rate was varied between 1 and 6 deg/s. In the case of the fixation of a ground plane element, a constant rotation rate was achieved by selecting an appropriate position of the fixation target on the plane. In the case of superimposed rotation, we intermixed rightward and leftward rotations. In addition, we also simulated movement through a cloud of dots with parameters similar to those used by Royden et al. (1992). The depth of the cloud ranged from 2 to 40 m, and the speed of the observer was 0.5 m/s. The resulting retinal flow is similar to the one depicted in Fig. 2c.

The results of the simulations can be seen in Fig. 4. Figure 4a shows the mean errors for the anisotropic network. For the ground plane with superimposed rotation and for the cloud, the error rises dramatically as the rotation rate increases. This is in agreement with the data of Royden et al. (1992). On the other hand, when the fixation of a ground plane element was simulated, the error remained low even with high rotation rates, consistent with the results of van den Berg (1993). The isotropic network yielded comparatively small errors for all three conditions, as can be seen in Fig. 4b.

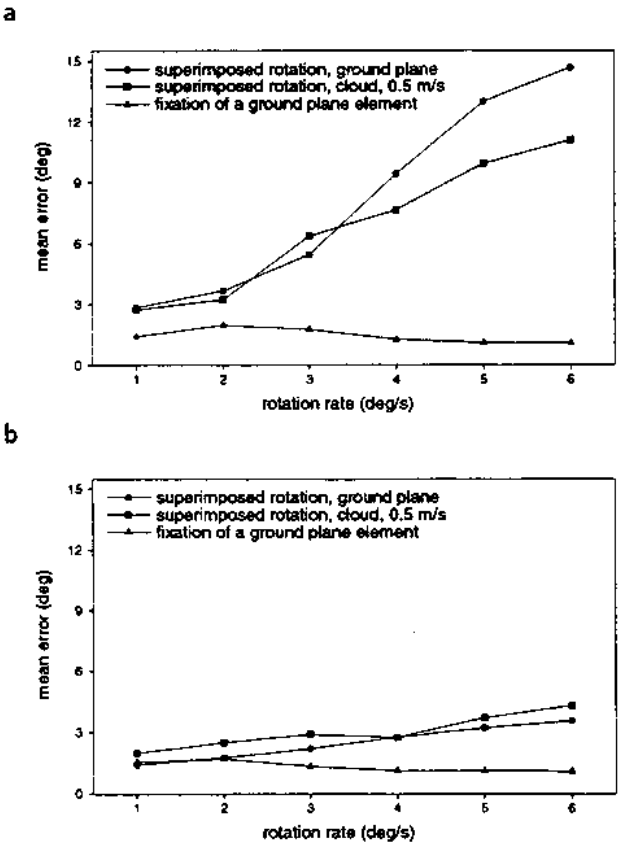

Fig. 4a, b. Comparison of the performance of the model under different eye-movement conditions. a Anisotropic distribution of direction preferences in the input layer. The network is biased towards centrifugal and circular retinal movements. No neurons with preferred directions towards the visual field center are included. The mean error in heading detection is plotted versus the eye rotation rate for three conditions. The first two conditions consist of a superimposed rotation around a vertical axis for movement either on top of a ground plane (condition one) or through a random cloud of dots (condition two). The third condition is movement over a ground plane while fixating a target that is rigidly attached to the plane. Corresponding examples of retinal flow fields can be seen in Figs. 1c, 2c, and 1b. Translational speed of the observer is 1.9 m/s in the two ground plane conditions and 0.5 m/s in the cloud condition. Conditions one and two yield very high errors as the rotation rate increases. Condition three, on the other hand, results in correct heading estimation for all rotation rates. b Same simulations as in a, but with an isotropic distribution of first-layer direction preferences. In this case, the simulations yield small errors for all three conditions

4.3 Variation of translational speed and rotation rate in a cloud-like environment

In Sect. 2.4, we pointed out that in an environment with a random depth structure, such as a cloud of random dots, the overall structure of the retinal flow depends on the relation between translational speed and the rotation rate. We therefore performed simulations in which the rotation rate was varied under a number of speed conditions. The results are depicted in Fig. 5. At a given rotation rate, the heading error is larger for small translational speeds than it is for high speeds. As expected, this dependency is especially pronounced when the network has an anisotropic distribution of preferences in the first

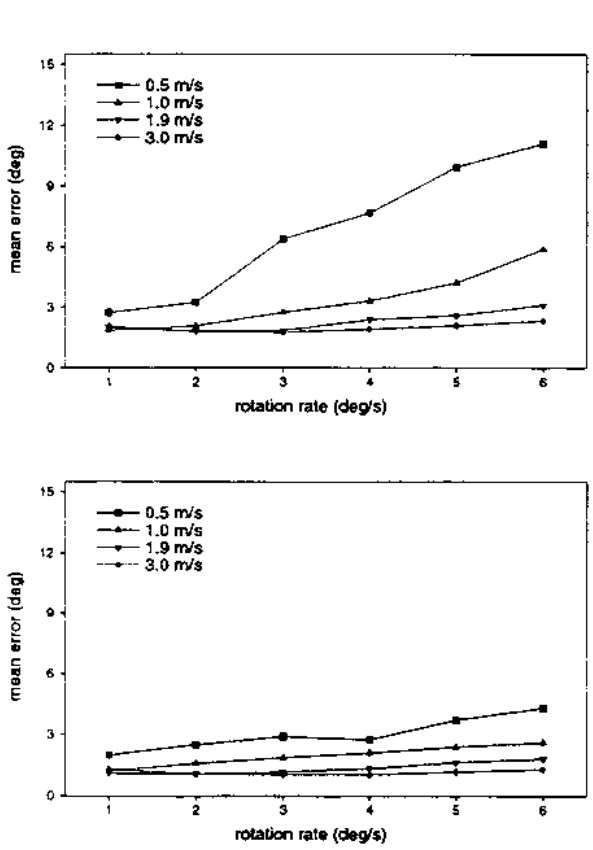

Fig. 5a, b. Mean heading error versus rotation rate for movements through a random cloud of dots at various translational speeds. Lower speeds result in a more lamellar retinal flow (see Fig. 2b, c for examples). **a** Anisotropic distribution of input direction preferences. Error depends on both the rotation rate and the translational speed. More lamellar flow fields result in larger errors. While at a speed of 0.5 m/s the error is very large, at speeds of 1.9 m/s and higher, it is only weakly influenced by the rotation rate. **b** Isotropic distribution of input direction preferences. The influence of the rotation rate on the heading error is minimal. Lamellar flow, however, still yields the largest error of all conditions tested

layer. However, the effect is also present in the isotropic network. It might thus be partly attributed to the flow pattern itself, indicating that for low speeds and high rotation rates, the flow becomes difficult to interpret. One has to keep in mind, however, that a speed of 0.5 m/s is a very slow pace and might indicate a situation in which accurate estimation of heading is usually not required.

The errors obtained with the cloud-like environment are usually somewhat larger than in the ground plane fixation condition, as a comparison between Figs. 4 and 5 shows. This is a general trend also reported for humans (van den Berg 1992; Warren and Hannon 1990).

At a speed of, e.g., 1.9 m/s, the mean error in the anisotropic network is comparatively low throughout the range of rotation rates tested. This is an interesting result given the structure of the retinal flow at higher rotation rates. To illustrate this, we have plotted the responses of the network to a single stimulation in Fig. 6. Figure 6a shows the retinal flow input to the network. The rotation rate is 5 deg/s. In Fig. 6b, the activities of the neurons in the first layer of the network are plotted. At each stimulated retinal location, a group of three neurons is present, the preferred directions of which are indicated by lines pointing away from the receptive field center. The activities of the neurons in response to the retinal flow from Fig. 6a are drawn as the lengths of these lines. Usually two neurons are activated at each location. In cases where the input flow vector is nearly parallel to one of the preferred directions, the activities of the neurons with preferred directions nearly orthogonal to the flow vector are too small to be seen. However, as there are no neurons with centripetal direction preference, flow vectors with a centripetal component always stimulate only one neuron. These movements will be incorrectly encoded by the first-layer populations. The resulting representation of the retinal flow by the first-layer neurons can be seen in Fig. 6c. In the right hemifield, the flow representation differs significantly from the real retinal flow depicted in Fig. 6a. However, the network is still able to find the correct direction of heading, as can be seen in Fig. 6d. In Fig. 6d, the activities of the second-layer populations are shown as a grey-scale map. Each square represents one specific direction of heading. Its grey level indicates the activity of the population which encodes this particular direction. The peak of activity is given by the brightest square and is close to the correct direction of heading, which is indicated by the cross.

4.4 Influence of the size of the visual field

The previous simulations have been performed with the size of the simulated visual field being equated to the size of the displays used in the psychophysical studies. However, visual field size is an important parameter for the computational analysis of retinal flow (Koenderink and van Doorn 1987). We therefore also performed simulations in which all parameters were identical to the simulation described in Sect. 4.2 and 4.3, but the diameter of the simulated visual field was increased to 80 deg. Figure 7 shows the results. In all simulations, the mean error was reduced compared with Sect. 4.2 (Fig. 5a) and 4.3 (Fig. 4a). Especially in the formerly critical situation of a superimposed vertical rotation during translation on top of a ground plane (Fig. 5a), the model is now able to retrieve the direction of heading when the visual field is unrestricted. On the other hand, the error for the translation of 0.5 m/s through the cloud is still very large, because the retinal flow in this situation stays lamellar also with the larger visual field size. As before, the errors for the cloud are generally larger than for the ground plane. Taken together, our model predicts that an increase in stimulus size should result in a decreased error in the ground plane condition but only weakly so in the cloud condition.

5 Discussion

In previous work, we proposed a network model of heading detection that captures some key properties of

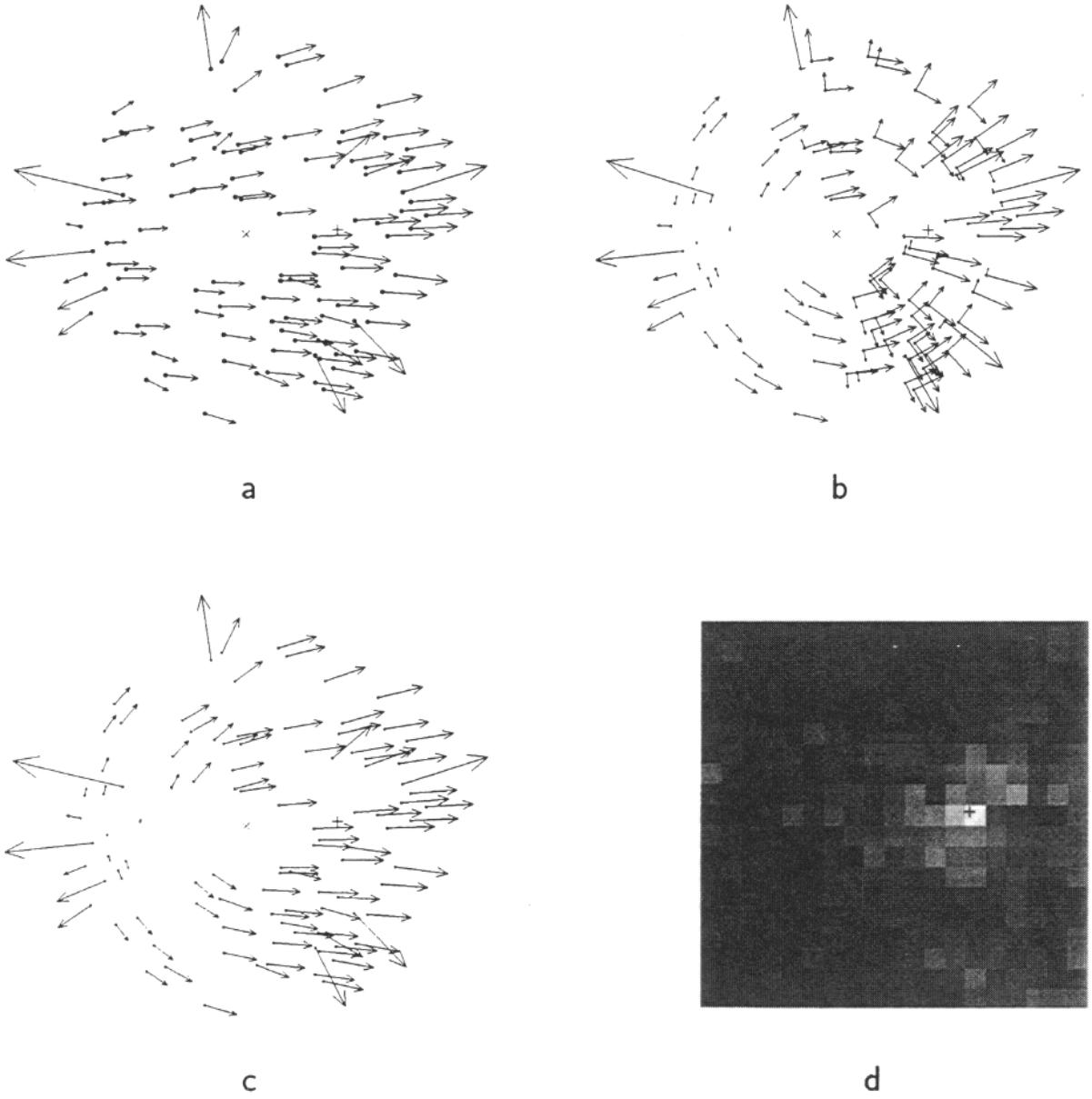

Fig. 6a–d. Example of a single simulation of the anisotropic network using a retinal flow field containing centripetal movement components. **a** Retinal flow input to the network. Movement through a random cloud of dots at a speed of 1.9 m/s with a superimposed eye rotation of 5 deg/s. **b** Activities of the first-layer neurons. Preferred directions are plotted as lines pointing away from the receptive field centers. Line lengths give the response activities. Notice that no neurons with centripetal direction preferences are present. **c** Partially incorrect representation of the retinal flow by the neuronal populations in the first layer due to the anisotropic distribution of direction preferences. In the right hemifield, the representation of the retinal flow differs significantly from the real retinal flow depicted in **a**. **d** Activities of the second-layer populations. Each square represents one direction of heading; its brightness corresponds to the population activity. Despite the incorrect encoding of the retinal flow in the first layer, the peak of activity (*brightest square*) is close to the correct direction of heading (+)

human psychophysics and at the same time generates cells with response properties similar to cells found in the MST area of the monkey visual cortex (Lappe and Rauschecker, 1993a, b). In the present paper, we presented a modified version of the model which incorporate motion detection anisotropies found in the visual cortical areas PMLS in the cat (Rauschecker et al. 1987) and MT in the monkey (Albright 1989; Lagae et al. 1993). The anisotropic model is able to reproduce seemingly conflicting recent psychophysical data and in doing so might aid in the understanding of the capabilities and constraints of the human heading detection system.

In the model, because of the anisotropic distribution of direction preferences, large heading detection errors occur when the retinal flow input contains many individual movements towards the fovea. This happens when

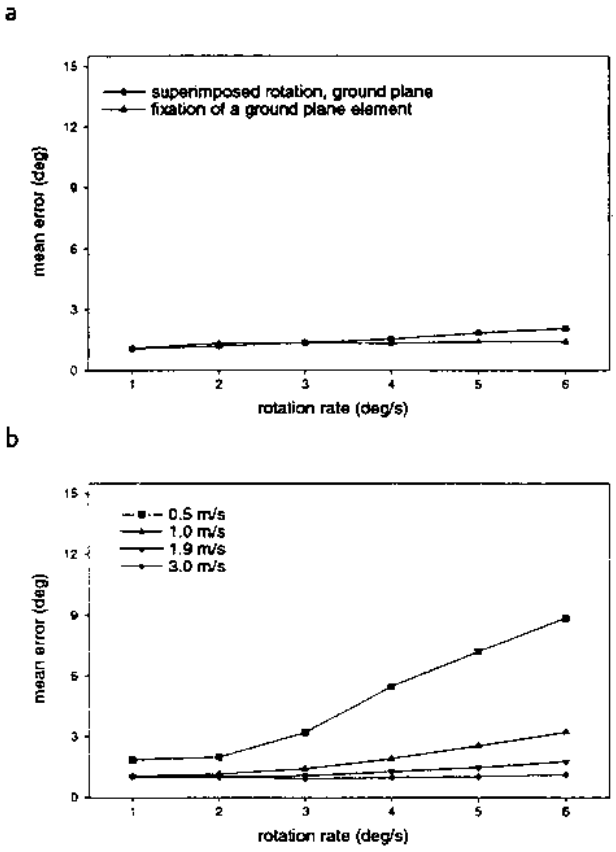

Fig. 7a, b. Mean heading error of the anisotropic network for various movements with a visual field diameter of 80 deg. **a** Movements on top of a ground plane as in Fig. 4. With the larger visual field size, the model yields comparatively low errors in both conditions. **b** Movements through a random cloud of dots as in Fig. 5. Throughout, the errors obtained with the 80 deg visual field are lower than those obtained with the 34-deg visual field. However, the error in the case of forward speed of 0.5 m/s is still large, and the anisotropic network cannot correctly recover the direction of heading in this situation

the observer moves on top of a ground plane and a constant eye rotation is superimposed on his movement, as in Fig. 1c. It does not occur, on the other hand, when the observer fixates a ground plane target while he is moving, although the amount of eye rotation may be identical in both cases (Fig. 1b). How can this difference be understood in an intuitive way? To construct the superimposed rotation stimulus of Fig. 1c, it is best to start out with the purely translational flow field of Fig. 1a. A rotation around a vertical axis alone, i.e. without any forward movement, results in a flow field that is approximately parallel to the horizon and independent of the distances of the points from the observer. If both movements are combined into one, the retinal flow is the mathematical superposition of the two individual flows, so that all flow vectors from Fig. 1a are approximately distorted by a common horizontal component. The result is the retinal flow depicted in Fig. 1c. For the case of the fixation of a ground plane element, on the other hand, the starting point is not the optic flow from Fig. 1a, but rather a shifted version of it, because now the observer gazes at some ground plane feature, which therefore is transformed into the center of the visual field. As the observer moves, he keeps his eyes fixed onto that environmental location. It is therefore intuitively clear that the visual field center must contain a fixed point. An eye rotation is necessary to keep the eyes fixed on the target. However, the axis of this eye rotation is not vertical in this situation. Instead, it is orthogonal to both the direction of heading and the direction of gaze. Since the environment is smooth (a plane), retinal motions around the fixed point in the center are small and increase with increasing retinal eccentricity. Under normal circumstances, the observer moves in a direction towards the fixated location, and the retinal motion is typified by an outflow from the fixation point. Now, what would happen if the fixation point were near the horizon, so that the axis of rotation would become vertical? In this case, the fixation point would be very far away from the observer. While the rotation axis would indeed be vertical, the rotation rate would be practically zero. The result is approximately a purely translational flow similar to the one depicted in Fig. 1a.

Movement on top of a ground plane while fixating stationary objects located at various distances and somewhere near the movement trajectory is probably the most common egomotion condition for ground-living mammals. We have shown that under these circumstances, the retinal flow vectors generally point away from the fovea, although there might be substantial local variations in direction. An arrangement of centrifugal and circular direction preferences of motion detectors, as found in cat area PMLS and monkey area MT, therefore seems to be a sensible design for the processing of these natural retinal flow fields.

An interesting point in this respect is that the centrifugal anisotropy is more pronounced in cat area PMLS than it is in monkey area MT. Besides the possible explanation that monkeys have a more elaborate visual system which is involved in more complex tasks in which centripetal motion would be important (e.g., reaching), this finding might also be related to the fact that cats are clearly more confined to the ground plane than macaques are and are probably even more often confronted with the centrifugal retinal flow pattern we described. On the other hand, in monkey area MT, several subpopulations of cells exist, and only some of these seem to carry the anisotropies (Lagae et al. 1993). It might be that only these cells are involved in the heading detection task. In humans, in turn, there is a psychophysical indication that centrifugal movements occurring during forward locomotion and centripetal movements are processed by two different systems (Mateeff et al. 1991; Perrone 1986).

Another aspect of the retinal flow pattern experienced during translation and fixation on a ground plane is that it partly resembles a spiraling motion around the fovea. Interestingly, many cells in the MST area of the macaque monkey that show responses to expanding and rotating flow patterns respond even better to spiraling patterns (Graziano et al. 1994). When we tested the model neurons in the second layer of our network with such spiraling

stimuli, they also turned out to be responsive to spiraling motions. With this in mind, we would like to emphasize once again that our model neurons are not constructed to yield specific response properties to certain flow patterns, but rather to serve in the computation of the direction of heading. The selectivities for expanding, rotating, or spiraling patterns are simply a consequence of their selectivity to heading direction.

Although the fixation of an environmental element might be the most common situation for humans, the ability to perform accurate heading detection may also be required during tracking of a moving target. This is a much more difficult task and seems to rely on extraretinal information about our eye movements (Royden et al. 1992). Extraretinal eye movement information can also be used in other situations that pose difficulties to the heading detection system, such as movement towards a frontoparallel plane (Warren and Hannon 1990). In what way the visual system might incorporate extraretinal eye movement information to serve as an additional cue about one's own motion is thus an important question that has to be pursued further (Lappe et al. 1994).

Several computational models for the visual detection of heading that bear on results from human psychophysics have been proposed (Hatsopoulos and Warren 1991; Hildreth 1992; Perrone 1992). The work we presented here, however, is different in that it directly relates observations at the neurophysiological level to results from psychophysical measurements in humans.

References

Albright TD (1989) Centrifugal directionality bias in the middle temporal visual area (MT) of the macaque. Visual Neurosci: 177–188

Ball K, Sekuler R (1980) Human vision favors centrifugal motion. Perception 9:317–325

Bauer R, Hoffmann K-P Huber HP, Mayr M (1989) Different anisotropies of movement direction in upper and lower layers of the cat's area 18 and their implications for global optic flow processing. Exp Brain Res 74:395–401

Berg AV van den (1992) Robustness of perception of heading from optic flow. Vision Res 32:1285–1296

Berg AV van den (1993) Perception of heading. Nature 365:497–498

Brenner E, Rauschecker JP (1990) Centrifugal motion bias in the cat's lateral suprasylvian visual cortex is independent of early flow field exposure. J Physiol 423:641–660

Bülthoff H, Little J, Poggio T (1989) A parallel algorithm for real-time computation of optical flow. Nature 337:549–553

Crowell JA, Banks MS (1993) Perceiving heading with different retinal regions and types of optic flow. Percep Psychophys 53:325–337

Cutting JE, Springer K, Braren PA, Johnson SH (1992) Wayfinding on foot from information in retinal, not optical, flow. J Exp Psych Gen 121:41–72

Duffy CJ, Wurtz RH (1991) Sensitivity of MST neurons to optic flow stimuli. I. A continuum of response selectivity to large-field stimuli. J Neurophysiol 65:1329–1345

Edwards M, Badcock DR (1993) Asymmetries in the sensitivity to motion in depth: a centripetal bias. Perception 22:1013–1023

Fahle M, Wehrhahn C (1991) Motion perception in the peripheral visual field. Graefes Arch Clin Exp Ophthalmol 229:430–436

Georgeson M, Harris MG (1978) Apparent foveofugal drift of counterphase gratings. Perception 7:527–536

Gibson JJ (1950) The perception of the visual world. Houghton Mifflin, Boston

Graziano MSA, Andersen RA, Snowden R (1994) Tuning of MST neurons to spiral motions. J Neurosci 14:54–57

Hatsopoulos NG, Warren WH Jr (1991) Visual navigation with a neural network. Neural Networks 4:303–318

Heeger DJ, Jepson A (1992) Subspace methods for recovering rigid motion. I. Algorithm and implementation. IJ Comp Vision 7:95–117

Hildreth EC (1992) Recovering heading for visually-guided navigation in the presence of self-moving objects. Philos Trans R Soc Lond Biol 337:305–313

Hildreth EC (1984) The measurement of visual motion. MIT, Cambridge, Mass

Koenderink JJ, Doorn AJ van (1981) Exterospecific component of the motion parallax field. J Opt Soc Am 71:953–957

Koenderink JJ, Doorn AJ van (1987) Facts on optic flow. Biol Cybern 56:247–254

Lagae L, Raiguel S, Orban GA (1993) Speed and direction selectivity of macaque middle temporal neurons. J Neurophysiol 69:19–39

Lappe M, Rauschecker JP (1993a) Computation of heading direction from optic flow in visual cortex. In: Giles CL, Hanson SJ, Cowan JD (eds), Advances in neural information processing systems 5. Morgan Kaufmann, New York

Lappe M, Rauschecker JP (1993b) A neural network for the processing of optic flow from egomotion in higher mammals. Neural Comp 5:374–391

Lappe M, Rauschecker JP (1994) Heading detection from optic flow. Nature 369:712–713

Lappe M, Bremmer F, Hoffmann K-P (1994) How to use non-visual information for optic flow processing in monkey visual cortical area MSTd. In: Marinaro M, Morasso PG (eds) ICANN 94-Proc Int Conf Artif Neur Netw Springer, Berlin Heidelberg New York

Longuet-Higgins HC, Prazdny K (1980) The interpretation of a moving retinal image. Proc R Soc Lond Biol 208:385–397

Marr D, Ullman S (1981) Directional selectivity and its use in early visual processing. Proc R Soc Lond Biol 211:151–180

Mateeff S, Yakimov N, Hohnsbein J, Ehrenstein WH, Bohdanecky Z, Radil T (1991) Selective directional sensitivity in visual motion perception. Vision Res 31:131–138

Maunsell JHR, Van Essen DC (1983) Functional properties of neurons in middle temporal visual area of the macaque monkey. I. Selectivity for stimulus direction, speed, and orientation. J Neurophysiol 49:1127–1147

Orban GA, Lagae L, Verri A, Raiguel S, Xiao D, Maes H, Torre V (1992) First-order analysis of optical flow in monkey brain. Proc Natl Acad Sci 89:2595–2599

Perrone JA (1986) Anisotropic responses to motion toward and away from the eye. Percept Psychophys 39:1–8

Perrone JA (1990) Simple technique for optical flow estimation. J Opt Soc Am [A] 7:264–278

Perrone JA (1992) Model for the computation of self-motion in biological systems. J Opt Soc Am [A] 9:177–194

Prazdny K (1980) Egomotion and relative depth map from optical flow. Biol Cybern 36:87–102

Rauschecker JP (1988) Visual function of the cat's LP/LS subsystem in global motion processing. Prog Brain Res 75:95–108

Rauschecker JP, Grünau MW von, Poulin C (1987) Centrifugal organization of direction preferences in the cat's lateral suprasylvian visual cortex and its relation to flow field processing. J Neurosci 7:943–958

Raymond JE (1994) Directional anisotropy of motion sensitivity across the visual field. Vision Res 34:1029–1037

Regan D, Beverly KI (1982) How do we avoid confounding the direction we are looking and the direction we are moving? Science 215:194–196

Reichardt W (1969) Movement perception in insects. In: Reichardt W (ed) Processing of optical data by organisms and machines. Academic Press, London, pp 465–493

Rieger JH, Toet L (1985) Human visual navigation in the presence of 3-D rotations. Biol Cybern 52:377–381

Royden CS, Banks MS, Crowell JA (1992) The perception of heading during eye movements. Nature 360:583–585

Saito H-A, Yukie M, Tanaka K, Hikosaka K, Fukada Y, Iwai E (1986) Integration of direction signals of image motion in the superior temporal sulcus of the macaque monkey. J Neurosci 6:145–157

Stoffregen TA (1985) Flow structure versus retinal location in the optical control of stance. J Exp Psychol Hum Percept Perform 11:554–565

Stoffregen TA (1986) The role of optical velocity in the control of stance. Percept Psychophys 39:355–360

Tanaka K, Saito H-A (1989) Analysis of motion of the visual field by direction, expansion/contraction, and rotation cells clustered in the dorsal part of the medial superior temporal area of the macaque monkey. J Neurophysiol 62:626–641

Tanaka K, Hikosaka K, Saito H-A, Yukie M, Fukada Y, Iwai E (1986) Analysis of local and wide-field movements in the superior temporal visual areas of the macaque monkey. J Neurosci 6:134–144

Uras A, Girosi F, Verri A, Torre V (1988) A computational approach to motion perception. Biol Cybern 60:79–87

Verri A, Aicardi F (1990) Limit cycles of the two-dimensional motion field. Biol Cybern 64:141–144

Verri A, Poggio T (1989) Motion field and optical flow: qualitative properties. IEEE Trans Patt Anal Mach Intell 11:490–498

Verri A, Girosi F, Torre V (1989) Mathematical properties of the two-dimensional motion field: from singular points to motion parameters. J Opt Soc Am [A] 6:698–712

Verri A, Straforini M, Torre V (1992) Computational aspects of motion perception in natural and artificial vision systems. Philos Trans R Soc Lond [Biol] 337:429–443

Wang HT, Mathur BP, Koch C (1989) Computing optical flow in the primate visual system. Neural Comp 1:92–103

Warren Jr WH, Hannon DJ (1988) Direction of self-motion is perceived from optical flow. Nature 336:162–163

Warren Jr WH, Hannon DJ (1990) Eye movements and optical flow. J Opt Soc Am [A] 7:160–169

Warren WH Jr, Kurtz KJ (1992) The role of central and peripheral vision in perceiving the direction of self-motion. Percept Psychophys 51:443–454

Werkhoven P, Koenderink JJ (1990) Extraction of motion parallax structure in the visual system I. Biol Cybern 63:185–191

Yuille AL, Grzywacz NM (1988) A computational theory for the perception of coherent visual motion. Nature 335:71–74